Impact of nonlinearities in multiple-antenna OFDM transceivers

Tim C.W. Schenk*‡, Peter F.M. Smulders* and Erik R. Fledderus*
* Eindhoven University of Technology, Radiocommunication Chair, PO Box 513, 5600 MB Eindhoven, The Netherlands
‡ Philips Research, High Tech Campus 27, 5656 AE Eindhoven, The Netherlands, tim.schenk@philips.com.

***Abstract*— This paper investigates the performance impact of nonlinearities in the transmitter (TX) as well as the receiver (RX) of multiple-antenna OFDM systems. First different, previously proposed, nonlinearity models are reviewed and their equivalence is shown. Subsequently, analytical expressions are derived for the probability of error of multiple-input multiple-output (MIMO) OFDM systems in Rayleigh-faded channels, which show good agreement with results from a simulation study. It can be concluded from the results that for high SNR values the TX nonlinearities cause performance floors, which are independent of the MIMO configuration. For RX nonlinearities, however, the performance in this high SNR region does depend on the MIMO configuration. The results can be used to derive limits for the permissible nonlinearities in MIMO OFDM systems.**

I. Introduction

The transfer experienced during a wireless transmission can in general be treated as linear, when conventional constant modulus signals are applied. Signals with high peak-to-average powers (like OFDM), on the other hand, likely experience nonlinearities in the different parts of the RF front-end, e.g., in the power amplifier and the low-noise amplifier. For a MIMO OFDM system, which requires multiple front-ends in both the TX and the RX of the system, the problem is more complicated as all transmission chains exhibit their own nonlinearity. Since the impact of nonlinearities can be significant for OFDM-based systems and remains unstudied for MIMO OFDM upto now, a careful investigation of the performance impact for such systems is justified and will be presented in this paper.

The influence of nonlinearities on the performance of conventional single-input single-output OFDM systems was earlier treated by several authors [1–5]. The work presented in [1], [3], [4] only regards a system experiencing an AWGN channel and TX nonlinearities. The work in [2] is limited to TX-based clipping for an OFDM system experiencing a wireless channel. Finally, the influence of TX clipping in a system experiencing either an AWGN or Rayleigh-faded channel is treated in [5]. The authors of [5], however, limit their analyses to the derivation of channel capacity and effective SNR.

The paper extends the work presented in these papers by regarding the influence of both TX- and RX-caused nonlinearities on the symbol-error rate (SER) performance of MIMO OFDM systems applying M-QAM modulation in Rayleigh-faded channels. The results are shown to be applicable for different previously presented memoryless nonlinearity models. The analysis is limited to amplitude-to-amplitude (AM-AM) nonlinearities, since for most amplifiers the influence of AM-AM distortion is dominant over that of amplitude-to-phase distortion. The paper separately regards the cases with TX and RX nonlinearities, modelling an uplink and downlink scenario, where the mobile station acts as TX and RX, respectively.

II. Nonlinearity modelling

In literature several baseband equivalent nonlinearity models are proposed, the most commonly used ones of which are the ideal clipping amplifier model, the travelling wave tube amplifier (TWTA) model of [6] and the solid state amplifier (SSA) model of [7]. Let us define $u = Ae^{j\phi}$ to be the baseband signal input to the nonlinearity $g(\cdot)$. Since for these AM-AM nonlinearities $g(u) = e^{j\phi}g(A)$, we can define the transfers of these three nonlinearities as

$$g_{\text{ideal}}(A) = \begin{cases} A & \text{for} \quad A \leq A_0, \\ A_0 & \text{for} \quad A > A_0, \end{cases} \tag{1}$$

$$g_{\text{TWTA}}(A) = \chi_{\text{A}} A/(1 + \kappa_{\text{A}} A^2), \tag{2}$$

$$g_{\text{SSA}}(A) = A/\big(1 + [A/A_0]^{2p}\big)^{\frac{1}{2p}}, \tag{3}$$

respectively. Here A_0 defines the amplifier saturation level, $\{\chi_{\text{A}}, \kappa_{\text{A}}\}$ are the parameters of the TWTA model and p defines the smoothness of the SSA model.

Another commonly used model is the odd-order polynomial model, defined by

$$g_{\text{poly}}(A) = \textstyle\sum_{n=0}^{N} \beta_{2n+1} A^{2n+1}, \tag{4}$$

where the model parameters β_n are real parameters for the here regarded AM-AM nonlinearities.

To show the equivalence between the above reviewed nonlinearity models, we derive the Taylor series expansions of the different AM-AM models under the assumption of small A. For the TWTA model, the result is given by

$$g_{\text{TWTA}}(A) = \chi_{\text{A}} A - \chi_{\text{A}} \kappa_{\text{A}} A^3 + \chi_{\text{A}} \kappa_{\text{A}}^2 A^5 + \mathcal{O}(A^7). \tag{5}$$

For the SSA model with $p \in \{1, 2, \ldots\}$ it yields

$$g_{\text{SSA}}(A) = A - \frac{1}{2pA_0^{2p}} A^{2p+1} + \frac{2p+1}{2(2p)^2 A_0^{4p}} A^{4p+1} + \mathcal{O}(A^{6p+1}). \tag{6}$$

The equivalence of (5) and (6) with (4), allows us to conclude that the TWTA and SSA can be modelled as a special case of the polynomial model.

To reveal the influence of nonlinearities on OFDM, we apply the findings of [8], which shows that for a Gaussian signal u input to a nonlinearity $g(\cdot)$ the output signal can be written as

$$u_{\text{d}} = g(u) = \alpha u + d, \tag{7}$$

where α is a scaling factor and d represents the distortion noise term, for which holds $d \sim \mathcal{CN}(0, \sigma_{\text{d}}^2)$ and $\mathbb{E}\{ud^*\} = 0$. Since the OFDM signal is approximately Gaussian for large number of subcarriers, we can also apply (7) for our analyses.

Since we have shown the equivalence between the polynomial, TWTA and SSA model, we only have to derive α and

0-7803-9785-1/06/$20.00

$\sigma_{\rm d}$ for the ideal clipping amplifier and the polynomial model to fully specify (7) for our problem. When the variance of u is defined as $2\sigma^2$, the results of the derivation are given by [9]

$$\alpha_{\rm poly} \;=\; \textstyle\sum_{n=0}^{N}\beta_{2n+1}2^n\sigma^{2n}\Gamma(2+n), \tag{8}$$

$$\alpha_{\rm ideal} \;=\; 1-\exp(-A_0^2/(2\sigma^2))+\tfrac{\sqrt{\pi}A_0}{\sqrt{2}\sigma}\,Q\left(A_0/\sigma\right), \tag{9}$$

where $\Gamma(\cdot)$ and $Q(\cdot)$ denote the Gamma- and Q-function, respectively. The variance of the distortion term is given by

$$\sigma_{\rm d}^2=\textstyle\int_0^\infty[g(A)]^2p(A)dA-2\alpha^2\sigma^2, \tag{10}$$

where $p(A)$ denotes the pdf distribution of A, which is Rayleigh distributed when $u\sim\mathcal{CN}(0,2\sigma^2)$.

III. System modelling

We can use these findings to reveal the influence of the nonlinearities on a MIMO OFDM system. Consider a system with $N_{\rm T}$ TX and $N_{\rm R}$ RX branches and $N_{\rm C}$ subcarriers. When we separately study TX and RX nonlinearities, the $N_{\rm R}N_{\rm C}\times1$ received frequency-domain signal vectors are given by [9]

$$\mathbf{x}_{\rm T} \;=\; \mathbf{H}(\mathbf{I}_{N_{\rm C}}\otimes\boldsymbol{\alpha}_{\rm T})\mathbf{s}+\mathbf{H}\mathbf{e}_{\rm T}+\mathbf{n}, \tag{11}$$

$$\mathbf{x}_{\rm R} \;=\; (\mathbf{I}_{N_{\rm C}}\otimes\boldsymbol{\alpha}_{\rm R})\mathbf{H}\mathbf{s}+\mathbf{e}_{\rm R}+\mathbf{n}, \tag{12}$$

respectively. Here the direct matrix product is denoted by $\otimes$, $\mathbf{I}_N$ is the N-dimensional identity matrix, $\mathbf{H}$ is the $N_{\rm R}N_{\rm C}\times N_{\rm T}N_{\rm C}$ block diagonal channel matrix and $\mathbf{s}$ denotes the $N_{\rm T}N_{\rm C}\times1$ frequency-domain TX vector, constructed as a stacking of the MIMO TX vectors for the different subcarriers. The receiver noise is modelled by the $N_{\rm R}N_{\rm C}\times1$ vector $\mathbf{n}$, the elements of which $\sim\mathcal{CN}(0,\sigma_{\rm n}^2)$. The $N_{\rm X}\times N_{\rm X}$ diagonal matrix $\boldsymbol{\alpha}_{\rm X}$ models the scaling due to the nonlinearities and is given by $\mathrm{diag}\{\alpha_1,\ldots,\alpha_{N_{\rm X}}\}$ for ${\rm X}\in\{{\rm T},{\rm R}\}$. The frequency-domain distortion noise is contained in the $N_{\rm T}N_{\rm C}\times1$ vector $\mathbf{e}_{\rm T}$ and the $N_{\rm R}N_{\rm C}\times1$ vector $\mathbf{e}_{\rm R}$, caused by TX and RX nonlinearities, respectively. Since the elements of $\mathbf{e}_{\rm T}$ and $\mathbf{e}_{\rm R}$ are the frequency-domain equivalents of d in (7), it is easily verified that they $\sim\mathcal{CN}(0,\sigma_{\rm e}^2)$, where $\sigma_{\rm e}^2=\sigma_{\rm d}^2$, i.e., the variance equals that of the time-domain distortion noise, as defined by (10).

When zero-forcing (ZF) based MIMO processing with perfect channel knowledge is applied to the received signal $\mathbf{x}$ in (11) and (12), we get

$$\tilde{\mathbf{s}} \;=\; \mathbf{H}^\dagger\mathbf{x}_{\rm T}=(\mathbf{I}_{N_{\rm C}}\otimes\boldsymbol{\alpha}_{\rm T})\mathbf{s}+\mathbf{e}_{\rm T}+\mathbf{H}^\dagger\mathbf{n}=\hat{\mathbf{s}}_{\rm T}+\boldsymbol{\varepsilon}_{\rm T}, \tag{13}$$

$$\tilde{\mathbf{s}} \;=\; \mathbf{H}^\dagger\mathbf{x}_{\rm R}=(\mathbf{I}_{N_{\rm C}}\otimes\boldsymbol{\alpha}_{\rm R})\mathbf{s}+\mathbf{H}^\dagger(\mathbf{e}_{\rm R}+\mathbf{n})=\hat{\mathbf{s}}_{\rm R}+\boldsymbol{\varepsilon}_{\rm R}, \tag{14}$$

respectively. Here † is the pseudo-inverse and the scaled TX vector is denoted by $\hat{\mathbf{s}}_{\rm X}=(\mathbf{I}_{N_{\rm C}}\otimes\boldsymbol{\alpha}_{\rm X})\mathbf{s}_{\rm X}$, for ${\rm X}\in\{{\rm T},{\rm R}\}$, and $\boldsymbol{\varepsilon}_{\rm T}=\mathbf{e}_{\rm T}+\mathbf{H}^\dagger\mathbf{n}$ and $\boldsymbol{\varepsilon}_{\rm R}=\mathbf{H}^\dagger(\mathbf{e}_{\rm R}+\mathbf{n})$ are the TX and RX nonlinearity-caused error vector. In (14) the assumption was made that α is branch independent, i.e., $\boldsymbol{\alpha}_{\rm R}=\alpha_{\rm R}\mathbf{I}_{N_{\rm R}}$

IV. Probability of error

The probability of erroneous detection can, subsequently, be derived in three steps. First the distribution of the effective SNR is derived. Subsequently, the SER in detection of $\hat{\rm s}$, for a given SNR value is calculated. Finally, the SER expressions are averaged over the SNR distribution. In the remainder we will derive the results for carrier k, the subvectors for which are denoted by the index (k) behind the vector. Since the statistics are equal for all k, the resulting probability of error can easily be generalised for all carriers later on.

A. TX nonlinearities

For TX nonlinearities, the mean of the $N_{\rm T}\times1$ error vector $\boldsymbol{\varepsilon}_{\rm T}$ for the kth carrier is given by $\boldsymbol{\mu}=\mathbb{E}\left[\boldsymbol{\varepsilon}_{\rm T}(k)\right]=\mathbf{0}$, since the elements of $\mathbf{n}(k)$ and $\mathbf{e}(k)$ possess zero mean. The $N_{\rm T}\times N_{\rm T}$ covariance matrix of the error in $\boldsymbol{\varepsilon}_{\rm T}(k)$, given the channel matrix $\mathbf{H}(k)$, is given by

$$\boldsymbol{\Omega}=\mathbb{E}\left[\boldsymbol{\varepsilon}_{\rm T}(k)\boldsymbol{\varepsilon}_{\rm T}^H(k)\big|\mathbf{H}(k)\right]=\sigma_{\rm e}^2+\sigma_{\rm n}^2\left(\mathbf{H}^H(k)\mathbf{H}(k)\right)^{-1}. \tag{15}$$

The covariance matrix of $\mathbf{s}_m$ equals $\sigma_{\rm s}^2\mathbf{I}$. The effective SNR for the kth carrier of the $n_{\rm T}$th TX branch is, consequently, given by

$$\wp_{n_{\rm T}}(k)=\left\{1/\wp_{{\rm T},n_{\rm T}}(k)+1/\wp_{{\rm R},n_{\rm T}}(k)\right\}^{-1}, \tag{16}$$

where we have defined the TX and RX SNR as

$$\wp_{{\rm T},n_{\rm T}}(k) \;=\; \sigma_{\rm s}^2/\sigma_{\rm e}^2, \tag{17}$$

$$\wp_{{\rm R},n_{\rm T}}(k) \;=\; (\sigma_{\rm s}^2/\sigma_{\rm n}^2)\left\{\left[\left(\mathbf{H}^H(k)\mathbf{H}(k)\right)^{-1}\right]_{n_{\rm T}n_{\rm T}}\right\}^{-1}, \tag{18}$$

respectively. Here $[\mathbf{A}]_{mm}$ denotes the mth diagonal element of matrix $\mathbf{A}$. When the channel matrix $\mathbf{H}(k)$ has i.i.d. complex Gaussian entries, $\wp_{{\rm R},n_{\rm T}}(k)$ is chi-square distributed with $2R=2(N_{\rm R}-N_{\rm T}+1)$ degrees of freedom. The pdf of $\wp_{{\rm R},n_{\rm T}}(k)$ is then given by

$$p_{\wp_{{\rm R},n_{\rm T}}(k)}(\rho)=\frac{(\rho/\wp_0)^{R-1}}{\wp_0(R-1)!}\exp\big(-\rho/\wp_0\big), \tag{19}$$

where $\wp_0$ is the average SNR, given by $\wp_0=\sigma_{\rm s}^2/\sigma_{\rm n}^2$.

When we, subsequently, want to calculate the probability of error of a system applying a rectangular M-QAM constellation and experiencing nonlinearities, we can use the observation from (13) and (14) that the estimated signal is given by a scaled version of the TX signal, denoted by $\hat{\mathbf{s}}_{\rm X}$, plus some error vector $\boldsymbol{\varepsilon}_{\rm X}$.

We will use this to derive the SER for the square M-QAM constellation based on that of a $\sqrt{M}$-PAM constellation. Since the real and imaginary part of the estimated symbols are independent, for a given SNR $\wp$ and scaling α and a zero-mean circularly symmetric complex Gaussian noise term, we can separately study the probability of error for the real and imaginary part of the signal. Since, moreover, the influence of α is identical for the real and imaginary part of the constellation, the expression for the SER can be written as

$$P^{\alpha}_{{\rm e},M\text{-QAM},E_{\rm s}}=1-\left(1-P^{\alpha}_{{\rm e},\sqrt{M}\text{-PAM},E_{\rm s}/2}\right)^2, \tag{20}$$

where $P^{\alpha}_{{\rm e},\sqrt{M}\text{-PAM},E_{\rm s}/2}$ denotes the probability of error for the α-scaled $\sqrt{M}$-PAM modulation with half the signal power of the corresponding QAM symbols.

As an example, the impact of the α-scaling on the 4-PAM constellation is schematically depicted in Fig. 1. In this figure, the originally transmitted 4-PAM constellation is depicted by dashed white dots and the scaled symbols are depicted by

black dots. It is clear that the distances to the decision boundaries, in dashed lines, are changed from the nominal $\sqrt{E_s/5}$ and that the shifts depend on the transmitted symbols. The figures shows that the shift is larger for the outer constellation points, i.e., s_1 and s_4. It is readily concluded from Fig. 1 that the shift for the nth constellation point s_n is given by $\delta_n = (\alpha - 1)s_n$. The distance to the decision boundaries are changed by δ_n, i.e., for half of the cases they are increased by δ_n and for the other half of the cases they are decreased by δ_n. For example for s_2, the distance to the left decision boundary at $-\sqrt{4E_s/5}$ is increased by $|(\alpha-1)s_2|$ and the distance to the right decision boundary at 0 is decreased by $|(\alpha-1)s_2|$.

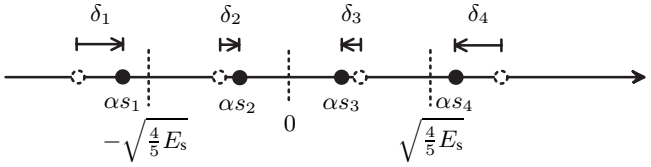

Fig. 1. Influence of α-scaling on the 4-PAM constellation points $\{s_1, ..., s_4\}$.

If we now additionally use that, by definition, the nth point of the N-PAM constellation, and the corresponding shift, are given by

$$s_n = \sqrt{3E_s/(N^2-1)}(2n-1-N), \quad (21)$$

$$\delta_n = \alpha s_n - s_n = (\alpha-1)\sqrt{\frac{3E_s}{N^2-1}}(2n-1-N), \quad (22)$$

respectively, we can derive the probability of symbol error for the α-scaled N-PAM constellation. We find that it is given by

$$P^{\alpha}_{\mathrm{e},N\text{-PAM},E_s} = \frac{1}{N}\left[\sum_{n=1}^{N/2}\left\{\mathbb{P}\left(|\varepsilon| > \frac{\sqrt{E_s}\beta_n^-}{c_1}\right) + \mathbb{P}\left(|\varepsilon| > \frac{\sqrt{E_s}\beta_n^+}{c_1}\right)\right\} - \mathbb{P}\left(|\varepsilon| > \frac{\sqrt{E_s}\beta_{N/2}^+}{c_1}\right)\right], \quad (23)$$

where $\beta_n^{\pm} = 1 \pm (1-\alpha)(2n-1)$, $c_1 = \sqrt{(N^2-1)/3}$ and ε denotes the element of the error vector for the kth carrier and n_Tth TX signal. By substituting (23) into (20), we find that

$$P^{\alpha}_{\mathrm{e},M\text{-QAM}} = 1 - \left(1 - \frac{2}{\sqrt{M}}\left\{\sum_{n=1}^{\sqrt{M}/2}\left(Q\left(\beta_n^-\sqrt{c_2\wp}\right) + Q\left(\beta_n^+\sqrt{c_2\wp}\right)\right) - Q\left(\beta^+_{\sqrt{M}/2}\sqrt{c_2\wp}\right)\right\}\right)^2, \quad (24)$$

where we defined $c_2 = 3/(M-1)$ and the SNR is given by $\wp = E_s/N_0$.

When we work out (24) for the special case of 4-QAM modulation, we find that the effect of the constellation scaling reduces to SNR scaling and that the SER is given by

$$P^{\alpha}_{\mathrm{e},4\text{-QAM}} = 2Q\left(\alpha\sqrt{\wp}\right) - \left[Q\left(\alpha\sqrt{\wp}\right)\right]^2 \approx 2Q\left(\alpha\sqrt{\wp}\right), \quad (25)$$

where the approximation is valid for large $\wp$.

Now, using the expression for the SNR $\wp$ in (16), and when we for readability omit the subcarrier and TX branch index, we can calculate the SER in a Rayleigh fading channel, which yields

$$P_e = \int_0^{\infty} P^{\alpha}_{\mathrm{e},M\text{-QAM}}\left(\frac{\wp_T\rho}{\wp_T+\rho}\right) p_{\wp_R}(\rho)d\rho. \quad (26)$$

For some special cases, we can derive a closed form solution for (26). For high values of $\wp_0$, we can make the following approximation $\left\{1/\wp_T + 1/\wp_R\right\}^{-1} \approx \wp_T = \sigma_s^2/\sigma_e^2$. Using this result, the SER in (26) is well approximated as

$$P_e \approx P^{\alpha}_{\mathrm{e},M\text{-QAM}}(\wp_T), \quad (27)$$

which for 4-QAM can be approximated by substituting (25) into (27), yielding $2Q(\alpha\sqrt{\wp_T})$. We note that (27) predicts the flooring in the SER curves depicted as a function of the SNR.

For low values of $\wp_0$, we can make the following approximation $\left\{1/\wp_T + 1/\wp_R\right\}^{-1} \approx \wp_R$. The SER expression in (26) is then well approximated by

$$P_e \approx \int_0^{\infty} P^{\alpha}_{\mathrm{e},M\text{-QAM}}(\rho)\, p_{\wp_R}(\rho)d\rho. \quad (28)$$

When we substitute (25) into (28), we find that for the low SNR region the SER approximation for a 4-QAM system in a Rayleigh fading channel is well approximated by

$$P_e \approx \frac{2(1-\sqrt{\wp_0 c_3})}{2}\ {}_2F_1\left(\frac{1}{2}, R+\frac{1}{2}; \frac{3}{2}; \frac{-\alpha^2\wp_0}{2}\right) \quad (29)$$

where $c_3 = \alpha\sqrt{\frac{2}{\pi}}\frac{(R-\frac{1}{2})!}{(R-1)!}$ and where ${}_2F_1(\cdot)$ denotes the hypergeometric function.

B. RX nonlinearities

For RX nonlinearities, the mean of the $N_t \times 1$ error vector for the kth carrier is given by $\boldsymbol{\mu} = \mathbb{E}[\boldsymbol{\varepsilon}_R(k)] = \mathbf{0}$, since the elements of $\mathbf{n}(k)$ and $\mathbf{e}(k)$ possess zero mean. The $N_t \times N_t$ covariance matrix of the error vector for the kth carrier is given by

$$\boldsymbol{\Omega} = \mathbb{E}\left[\boldsymbol{\varepsilon}_R(k)\boldsymbol{\varepsilon}_R^H(k)\middle|\mathbf{H}(k)\right] = (\sigma_e^2+\sigma_n^2)\left(\mathbf{H}^H(k)\mathbf{H}(k)\right)^{-1}, \quad (30)$$

where we recall that $\sigma_e^2 = \sigma_d^2$, as derived for different nonlinearities in Section II. The effective SNR for the kth carrier of the n_tth TX branch is, consequently, given by

$$\wp_{n_t}(k) = (\sigma_s^2/(\sigma_e^2+\sigma_n^2))\left\{\left[\left(\mathbf{H}^H(k)\mathbf{H}(k)\right)^{-1}\right]_{n_T n_T}\right\}^{-1}. \quad (31)$$

When the experienced channel exhibits complex Gaussian fading, $\wp_{n_t}(k)$ is distributed according to the chi-square distribution with $2R$ degrees of freedom, the pdf of which is given by (19). Here the average SNR $\wp_0 = \sigma_s^2/(\sigma_e^2+\sigma_n^2)$.

For a given SNR, the probability of erroneous symbol detection of an M-QAM symbol in $\hat{\mathbf{s}}(k)$ is given by $P^{\alpha}_{\mathrm{e},M\text{-QAM}}$, which was found to be given by (24). Using the expression for the effective SNR $\wp$ in (31), and when we omit the subcarrier and TX branch index, we find the resulting SER is given by

$$P_e = \int_0^{\infty} P^{\alpha}_{\mathrm{e},M\text{-QAM}}(\rho)p_{\wp}(\rho)d\rho. \quad (32)$$

For the special case of 4-QAM modulation, (32) can be approximated by substituting (25) into (32), which yields (29), though with $\wp_0$ as defined in this section.

V. Numerical results

The derived analytical symbol-error rate expressions are in this section compared with results from Monte Carlo simulations of a system with N_C = 1024 subcarriers, applying 16-QAM modulation and no coding. The channel is modelled to be i.i.d. Rayleigh-faded over space and frequency. The clipping amplifier of (1) is used as nonlinearity. All results are given as function of average SNR, defined as $N_T\sigma_s^2/\sigma_n^2$.

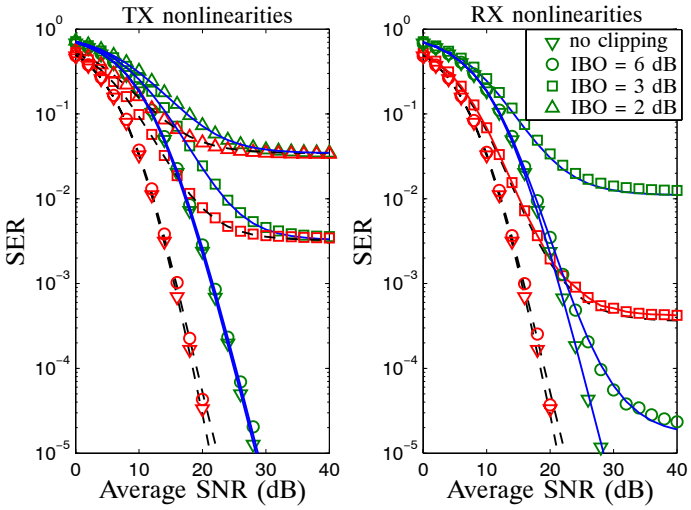

Fig. 2. SER performance of systems experiencing TX or RX nonlinearities and a Rayleigh-faded channel. Results are depicted for an 1×4 (dashed lines) and 2×4 (solid lines) 16-QAM system. Analytical results are in lines and simulation results are depicted by markers.

The SER results are depicted in Fig. 2 for an 1×4 (dashed lines) and 2×4 (solid lines) system, where analytical results are in lines and simulation results are depicted by markers. The results are given for different values of input backoff (IBO = $A_0^2/(2\sigma^2)$) to the nonlinearities. It can be concluded that there is a good agreement between the analytical and simulation results. At high SNR values the nonlinearity-caused distortion noise becomes dominant and flooring occurs for both TX and RX nonlinearities. For the TX nonlinearities this flooring is independent of the MIMO configuration, which is not the case for RX nonlinearities, as was predicted from the analytical study. This is intuitively explained by the location where the additive distortion source occurs for the two types of nonlinearities, i.e., in front or behind the channel. As such the impact of RX nonlinear distortion does depend on the dimensions of the channel matrix, while that of the TX nonlinearities is independent of the MIMO system dimensions.

Fig. 3 further investigates the analytical SER expressions in (26) and (32). Different MIMO configurations are considered, all with IBO = 3 dB. Again, it can be concluded that the SER flooring for TX nonlinearities does not depend on the MIMO configuration, while it does for RX nonlinearities. Hence, a system experiencing RX nonlinearities benefits from the spatial diversity provided by the MIMO channel, i.e., the influence of the nonlinearities is reduced by using a higher number of RX antennas. For symmetric systems, i.e., $N_T = N_R$, TX nonlinearities are less severe than RX nonlinearities.

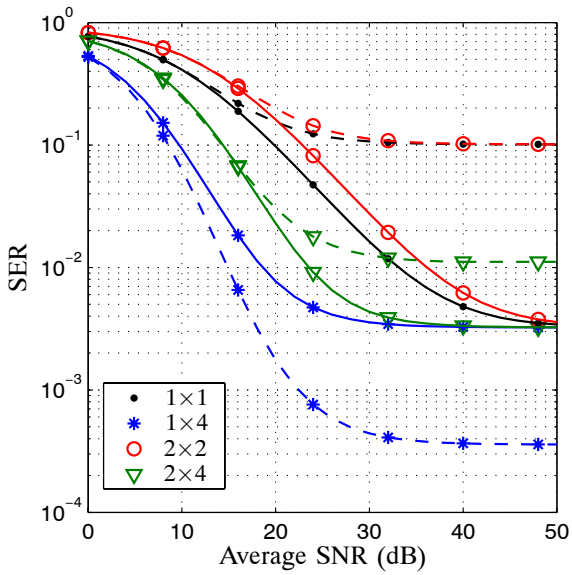

Fig. 3. Comparison of the analytical SER results for TX nonlinearities in (26) (solid lines) and RX nonlinearities in (32) (dashed lines) for different 16-QAM MIMO systems. Clipping amplifiers with IBO = 3 dB are used.

VI. Conclusions

The influence of both TX and RX nonlinearities on the performance of a multiple-antenna OFDM system was analyzed in this paper. Both the error in detection and the SER performance were derived for Rayleigh-faded channels. A difference in the impact between TX and RX nonlinearities is observed, which can be attributed to the location in the transmission chain of distortion noise term. Therefore TX nonlinearities cause an irreducible SER floor independent of the MIMO configuration and RX nonlinearities cause flooring dependent on the difference of the number of TX and RX branches.

References

[1] E. Costa, M. M. Midrio, and S. Pupolin, "Impact of amplifier nonlinearities on OFDM transmission system performance," *IEEE Commun. Letters*, vol. 3, pp. 37–39, Feb. 1999.

[2] X. Li and L. J. Cimini, "Effects of clipping and filtering on the performance of OFDM," *IEEE Commun. Letters*, vol. 2, pp. 131–133, May 1998.

[3] P. Banelli, "Theoretical analysis and performance of OFDM signals in nonlinear AWGN channels," *IEEE Trans. on Commun.*, vol. 48, pp. 430–441, Mar. 2000.

[4] D. Dardari, V. Tralli, and A. Vaccari, "A theoretical characterization of nonlinear distortion effects in OFDM systems," *IEEE Trans. on Commun.*, vol. 48, pp. 1755–1764, Oct. 2000.

[5] H. Ochiai and H. Imai, "Performance analysis of deliberately clipped OFDM signals," *IEEE Trans. on Commun.*, vol. 50, pp. 89–101, Jan. 2002.

[6] A. A. M. Saleh, "Frequency-independent and frequency-dependent nonlinear models of TWT amplifiers," *IEEE Trans. on Commun.*, vol. COM-29, pp. 1715–1720, Nov. 1981.

[7] C. Rapp, "Effects of HPA-nonlinearities on a 4-DPSK/OFDM-signal for a digital sound broadcasting system," in *Proc. second European conference on Satellite Communication, Liege, Belgium*, Oct. 1991, pp. 179–184.

[8] J. J. Bussgang, "Crosscorrelation functions of amplitude-distorted Gaussian signals," Tech. Rep. 216, Research Lab. Electron, M.I.T., Cambridge, MA, Mar. 1952.

[9] T. C. W. Schenk, *RF Impairments in Multiple Antenna OFDM: influence and mitigation*, Ph.D. thesis, Eindhoven University of Technology, Nov. 2006.